Integrating GM and XROMM illuminates the role of the quadrate as a keystone of cranial kinesis

Miranda Margulis-Ohnuma

Advisors: Anjan Bhullar and Armita Manafzadeh

Second Reader: Jacques Gauthier

13 December 2023

A Senior Thesis presented to the faculty of the Department of Earth and Planetary Sciences, Yale University, in partial fulfillment of the Bachelor of Science Degree.

ABSTRACT

Modern birds are a highly successful and diverse clade and possess a variety of unique morphological innovations of the skeleton. Among these is the avian cranial kinetic apparatus, which allows the upper beak to move independently of the lower jaw, creating opportunities for diverse functional beak mobility. Biomechanical technology and paleontological discovery are advancing in parallel, furthering our understanding of the form-function relationship in modern birds and of the origins of distinctive avian morphologies in the fossil record. Here, we integrate *in vivo* XROMM data with 3D geometric morphometric analysis of bird-line fossils to assess the functional significance of evolutionary trends in morphology and to illuminate the origin of the modern cranial kinesis mechanism. We find that the articulations between the quadrate and its surrounding bones – the quadratojugal, mandible, and squamosal – evolved significantly throughout the avian lineage even prior to the sudden transformation to the modern quadrate seen in ornithurines. In particular, a reduction of total quadrate-quadratojugal contact, variation on the ancestrally bicondylar mandibular joint, and the origin of a bicondylar joint at the otic articulation are innovations of form that enabled innovations of function.

INTRODUCTION

Avian Cranial Kinesis

Cranial kinesis, the movement of internal skull bones with respect to one another, is well known in many vertebrates. Mechanisms for kinesis vary among vertebrate taxa (Wilken et al., 2020), from the premaxillary/maxillary swing of suction-feeding fish (Westneat, 2005) to the hyperkinetic gape of snakes (Kardong, 1977). The unique cranial kinetic apparatus of birds is an ancestral key innovation of the clade. Beak mobility, enhanced by kinesis, enables widespread

ecological success and diverse specialization among modern birds (Zweers & Berkhoudt, 2001). However, the evolutionary origin of this functionally significant avian trait is opaque. The fossil record shows an abrupt transformation from primitive to nearly modern morphologies and configurations of skeletal elements involved in the kinetic system.

Within the extreme diversity of modern birds, there are modifications to and variations on the underlying streptostylic mechanism. In general, the upper jaw is mobile relative to the rest of the skull through two main types of cranial kinesis: prokinesis and rhynchokinesis (Zusi, 1984). Both types involve movement of the quadrate, jugal bar, and pterygoid-palatine complex, but differ in the main axis of rotation, with prokinesis occurring within a small bending zone or hinge in the proximal part of the beak whereas rhynchokinesis occurs either centrally or distally. In a functional sense, the effects are broadly similar (Gussekloo et al., 2001). Models have shown that biomechanical diversity exists within rhynchokinesis, with neognath beaks possessing clear bending zones while bending occurs along the entire beak in paleognaths (Gussekloo & Bout, 2005). The avian kinetic mechanism has traditionally been modeled as a system of inflexible bars connected by pin hinges (Zusi, 1984), a simplification which underlies our basic understanding of the apparatus, but which is rapidly being contradicted by new evidence. For instance, more detailed work on the anatomy of the otic, mandibular, and palatobasal joints in ducks using histology shows that these three joints are synovial and bichondral, with articular cartilage on both surfaces (Bailleul et al., 2016), suggesting the potential for more complex, three-dimensional joint motion.

Work on modern birds, especially involving live animals, has historically been limited to external observations of feeding behavior. Gussekloo et al. (2001) used stereophotogrammetry to analyze bone displacement during cranial kinesis in five species with diverse skull morphologies,

establishing our basic understanding of the system's general dynamics: quadrate motion is transferred by the jugal bar and pterygoid-palatine complex to the upper bill, restricting kinesis to the antero-posterior plane. Further video imaging experiments using the paleognath *Rhea americana* aimed explicitly to explore the connection between feeding behavior and palate morphology, but found no significant functional relationship (Gussekloo & Bout, 2005). However, new technology that uses X-ray imaging to generate accurate and precise 3D animations of *in vivo* kinematics is rapidly transforming our potential to understand internal biomechanics (Brainerd et al., 2010). X-ray Reconstruction of Moving Morphology (XROMM) has been used to experimentally investigate form-function relationships in a variety of vertebrate taxa, from locomotion (e.g., Tsai et al., 2019) to feeding (e.g., Weller et al., 2020; Bhullar et al., 2019). In one of the first published XROMM studies, Dawson et al. (2011) used this approach to study the kinematics of cranial kinesis in ducks, revealing motion in three dimensions and bone deformation during kinesis, both of which contradict the assumptions of the traditional avian kinesis model. Going forward, further XROMM experiments are the key to more thoroughly understanding the relationship between skeletal morphology and kinetic potential.

A parallel line of research has used fossil data to investigate the evolutionary history of the morphology involved in the avian kinetic apparatus. Previous studies have attempted to characterize fossils on the avian stem as kinetic or akinetic based on hypothesized prerequisite anatomy for kinesis, regardless of overall similarity to the modern mechanism. The Late Cretaceous ornithurines *Hesperornis* and *Parahesperornis* demonstrate skull element morphologies consistent with a modern avian kinetic mechanism: a streptostylic quadrate bone with a modern otic joint articulation, three types of flexion zones, and a rigid upper jaw are evidence of prokinesis in *Hesperornis* and *Parahesperornis*, supporting prokinesis as the

ancestral type of avian cranial kinesis (Buhler et al., 1988). Buhler and colleagues also characterized the skull of *Hesperornis* as conforming to a modern modular layout of four kinematic units, the upper jaw, lower jaw, palate, and braincase. Further down the stem, the akinetic skull of Early Cretaceous enantiornithine *Yuanchuavis* suggests a mosaic assembly of the prerequisite anatomy for cranial kinesis, beginning with transformations to the palate (Wang et al., 2022). Despite distinctly primitive morphologies of components involved in the modern mechanism, the alvarezsaurid *Shuvuuia* has also been suggested to possess prokinetic capacity on the basis of its overall quadrate morphology, its thinning of the jugal bar, and its noncontinuous naso-orbital septum (Chiappe et al., 1998). Intracranial mobility has further been proposed in other dinosaurs, long before the evolution of the morphologically modern apparatus, but Holliday and Witmer (2008) found that, while some prerequisites of cranial kinesis (synovial otic and basal quadrate joints and protractor musculature) were present in dinosaurs, the kinematic linkages necessary for cranial kinesis were absent in dinosaur skull morphology. Bhullar et al. (2016) highlighted the role of paedomorphosis as a developmental mechanism for the evolution of kinetic anatomy. Understanding the relative timing and integration of the evolution of components involved in modern avian cranial kinesis is essential to uncovering its functional origins.

Avian cranial kinesis remains a biomechanical and evolutionary mystery, despite its biological importance and despite significant research interest. Documenting the evolutionary history of this key functional innovation requires a thorough examination of its origins in the fossil record combined with an analysis of the relationship between its form and function. Here, we synthesize biomechanical function-focused and paleontological form-focused methods to establish a clearer understanding of the avian cranial kinesis mechanism.

Evolution of the Quadrate, the Keystone of Kinesis

The major skeletal components of the modern avian kinetic mechanism are the neurocranium, upper beak, jugal bar, and quadrate, all of which move relative to one another. Of these, the quadrate is most enigmatic and likely most significant, as it is the locus of initiation for kinetic movement and therefore has been called a "keystone" of cranial kinesis (Dawson et al., 2011). An element of the endochondral splanchnocranium, the quadrate provides the articulation between the skull and lower jaw in all postembryonic jawed vertebrates except mammals, in which it is transformed during early development into the incus, a bone of the middle ear (Hendrickx et al., 2015). The avian quadrate bone articulates with the neurocranium at the otic joint at its posterodorsal extent, with the jugal bar on its lateral surface, with the pterygoid at its anteromedial extent, and with the mandible at its ventral surface, forming the lower jaw joint (Fig. 1). The protractor muscle (M. protractor pterygoidei et quadrati) attaches broadly to the dorsal edge of the orbital process (Bhattacharyya, 2013). As a locus of attachment for bones and muscles involved in cranial kinesis, the quadrate has a complex three-dimensional structure apparently sculpted by functional selection.

However, the diversity of quadrate morphologies in modern birds remains largely unstudied (Fig. 2). Only one analysis, published earlier this year, has quantified the three-dimensional morphology of avian quadrates; this study focused on the evolution of the galloanseran quadrate, incorporating fossil evidence to reconstruct the ancestral galloanseran condition (Kuo et al., 2023). The functional significance of quadrate anatomical variation and its relationship to cranial kinesis remains unknown, as well as the extent to which disparity represents an ecological versus a phylogenetic signal.

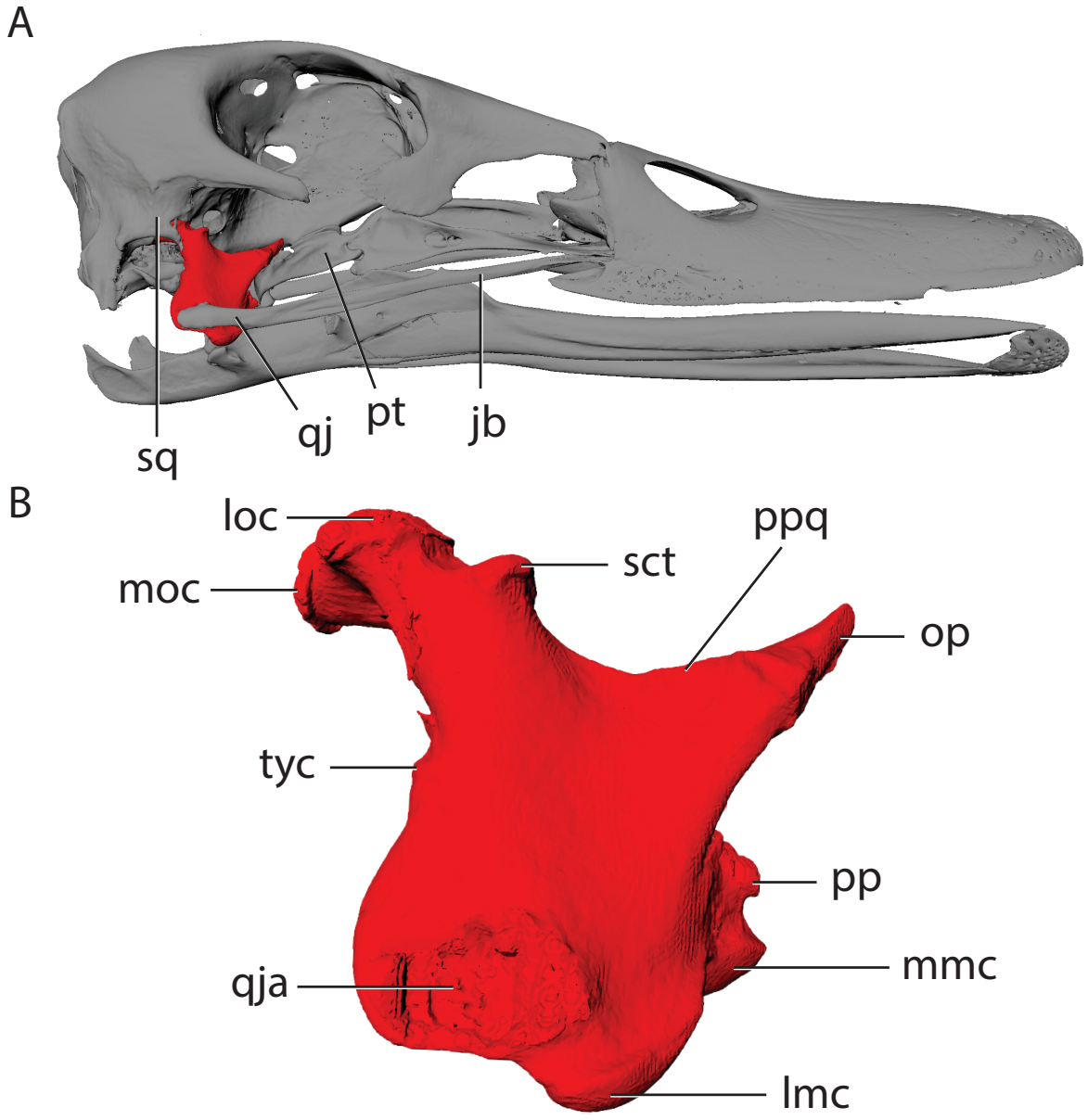

Fig. 1: The quadrate is notable for its many articulations with surrounding bones and muscles, as seen in the full duck skull (A) and in quadrate anatomy (B). Abbreviations: jb, jugal bar; lmc, lateral mandibular condyle; loc, lateral otic condyle; moc, medial otic condyle; mmc, medial mandibular condyle; op, orbital process; pp, pterygoid process; ppq, insertion of the M. protractor pterygoidei et quadrati; pt, pterygoid; qj, quadratojugal; qja, quadratojugal articulation; sct, subcapitular tubercle; sq, squamosal; tyc, tympanic crest.

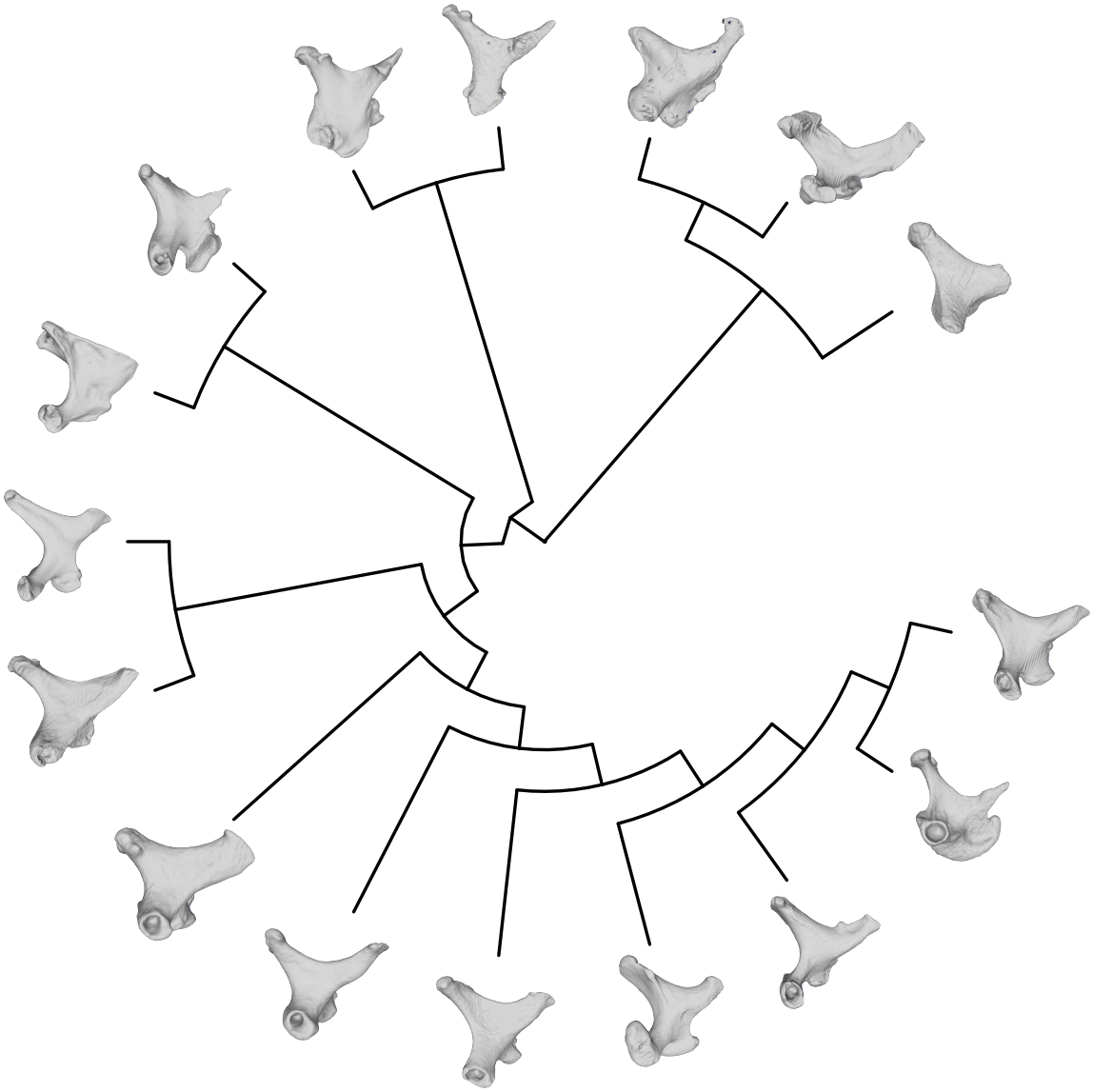

Fig. 2: Disparity of modern bird quadrates used in this study. Counterclockwise from top right: *Struthio camelus*, *Apteryx australi*, *Crypturellus undulatu*, *Gallus varius*, *Anas platyrhynchos*, *Podargus strigoides*, *Colibri coruscans*, *Hierococcyx fugax*, *Columba livia*, *Aramus guarauna*, *Eurypyga helias*, *Pandion haliaetus*, *Colius macrourus*, *Chunga burmeisteri*, *Nestor notabilis*, *Menura novaehollandiae*.

This morphological perspective on quadrate evolution allows for the use of fossil data. In the bird-line fossil record, the abrupt origin of the modern kinetic apparatus is most strikingly indicated by a sudden transformation of the quadrate, leading to a clear distinction between the "ancestral" and "derived" forms (see Fig. 3C). Though homologous features can be identified between ancestral-state and derived-state quadrates, their drastic qualitative differences have led to two sets of terminology, which obscures our conceptualization of the continuous evolutionary process connecting the old form to the new (Hendrickx et al., 2015). However, a broader characterization of archosaur quadrate evolution prior to and following the gap in the fossil record may illuminate the trajectories of evolution that ultimately led to the modern cranial kinetic mechanism.

In this paper, we aim to shed light on the origin of the avian cranial kinetic mechanism by quantifying morphological evolution of the quadrate and considering quadrate features from a functional perspective. Through integration of data from extinct and extant animals, we take a new approach to this classic biomechanical and evolutionary problem.

METHODS

Both methods used in this study, XROMM and geometric morphometrics, simplify complex anatomical structures to a series of points in three-dimensional space. The relative positions of these points can then be analyzed to understand either motion or evolution of shape.

X-Ray Reconstruction of Moving Morphology (XROMM)

To produce a clear visualization of the motion and morphological interactions involved in cranial kinesis, we re-analyzed the only avian skull XROMM dataset to date, which captures duck feeding behavior (Dawson et al., 2011). This dataset was collected at Brown University and

made available to our lab by Dr. Elizabeth Brainerd. We employed the software XMALab, developed after the publication of the original study, to retain more information from the raw data (Knörlein et al., 2016). The skull contained a total of 18 radiopaque markers: three each in the braincase, jugal, and quadrate, four in the upper beak, and five in the mandible. We manually tracked the 3D position of these makers through 2047 two-dimensional images to produce a clear visualization of bone motion. Markers in each bone were grouped into a rigid body unit, then rigid body transformations were filtered at 25 Hz and exported for use in animation.

We also digitally segmented a microCT scan of this duck, using its anatomy to make morphologically accurate reconstructions of skull elements and their articulations, and using the positions of its radiopaque XROMM markers to calculate rigid body transformations in XMALab. The duck used in this experiment was microCT scanned by Dr. Matthew Colbert at the University of Texas High-Resolution X-ray CT Facility in January 2008, generating a high-resolution grayscale TIFF stack. We segmented the neurocranium, upper beak, jugal bar, quadrate, and mandible in the software package VGStudio Max 2023 (Volume Graphics) by digitally tracing the edges of the bones to create an individual region of interest (ROI) representing each element. Our resulting three-dimensional models were more precise than those used in the original study, which were generated using global thresholding rather than anatomically informed segmentation (Dawson et al., 2011).

Using the 3D animation software Autodesk Maya, we generated a visualization that captures both the movement and the morphology of the elements involved in kinesis by applying the rigid body motion data calculated through XROMM tracking to the bone models created through segmentation. The animation is an intermediate product that serves as raw data for biomechanical analysis of the joints involved in kinesis, particularly motion of the quadrate

relative to the neurocranium at the otic joint. Joint coordinate systems at the nasofrontal hinge, jaw joint, and otic joint were calculated by assigning anatomical coordinate systems based on the anatomy of segmented elements, following Dawson et al. (2011). Kinematics – in this case, the relative timing and excursions of rotations in three degrees of freedom – were measured from each joint coordinate system using Maya's Graph Editor.

Geometric Morphometrics (GM)

In parallel, we used a 3D geometric morphometric analysis to investigate morphological change in the quadrate over the course of avian evolution. GM is a widely used framework for quantitatively comparing shape that extracts information about overall morphology by mathematically describing the relative positions of biologically homologous points called "landmarks" (Zelditch et al., 2004). Landmark digitization and all analyses were conducted using the R package "geomorph" (Adams & Otárola-Castillo, 2013).

Sampling and Data Acquisition

Since we wanted to understand the overall evolutionary trajectory of avian quadrate evolution, our sample includes the quadrates of both fossil and extant organisms. To capture the vast disparity of crown bird quadrate morphology, our modern sample includes a specimen from every major clade of the comprehensive bird phylogeny published by Prum et al. (2015) (Fig. 6B). In addition, we included a parrot (*Nestor notabilis*), a group known for having extreme cranial kinesis ability, and a total of three paleognaths rather than one because of this clade's morphological diversity and atypical mode of kinesis. Modern bird datasets were either directly downloaded as 3D models from MorphoSource, segmented from CT data downloaded from MorphoSource, or segmented from CT data collected at Yale, for a total of sixteen modern avian

datasets (Table 1). Extant reptile outgroup datasets (tuatara, iguana, gecko, alligator) were also downloaded from MorphoSource.

Fossil datasets spanning archosaur evolution were chosen based on phylogenetic position, data availability, and quality of 3D quadrate preservation. The nine included fossil datasets represent evolution from the early archosauromorph *Prolacerta* to ornithurines *Ichthyornis* and *Hesperornis* (Table 1) (Fig. 6B). The better-preserved (left or right) quadrate was chosen for each fossil, with data collected from left quadrates subsequently reflected such that all landmark coordinates correspond to right quadrates. Other than *Majungasaurus*, from MorphoSource, all fossil datasets were collected by members of the Bhullar Lab at Yale and used with permission.

Table 1: Taxon sampling used in this study.

Species	Category	Source	Access/Preparation	Side	Preparation Needed
Alligator mississippiensis	extant outgroup	MorphoSource	Ohio University Vertebrate Collection	right	none
Anas platyrhynchos	extant bird	MorphoSource	UMZC Zoological Specimens	right	none
Apteryx australis	extant bird	MorphoSource	Field Museum of Natural History Bird Collection	right	none
Aramus guarauna	extant bird	MorphoSource	Field Museum of Natural History Bird Collection	right	none
Chunga burmeisteri	extant bird	MorphoSource	Field Museum of Natural History Bird Collection	right	none
Colibri coruscans	extant bird	MorphoSource	Field Museum of Natural History Bird Collection	right	none
Colius macrourus	extant bird	MorphoSource	Field Museum of Natural History Bird Collection	right	none
Columba livia	extant bird	MorphoSource	Field Museum of Natural History Bird Collection	right	none
Crypturellus undulatus	extant bird	MorphoSource	Natural History Museum (London) Collection Specimens	right	segmented from CT data
*Eosphorosuchus lacrimosa**	fossil	Bhullar Lab	Miranda Margulis-Ohnuma	right	segmented from CT data
Euparkeria capensis	fossil	Bhullar Lab	Caleb Gordon	left	none
Eurypyga helias	extant bird	MorphoSource	Field Museum of Natural History Bird Collection	right	none
Gallus varius	extant bird	MorphoSource	Natural History Museum (London) Collection Specimens	right	segmented from CT data
Gracilisuchus stipanicicorum	fossil	Bhullar Lab	Caleb Gordon	right	none
Hemidactylus turcicus	extant outgroup	MorphoSource	FLMNH Division of Herpetology	right	none
Hesperornis regalis	fossil	Bhullar Lab	Michael Hanson	left	none
Hierococcyx fugax	extant bird	MorphoSource	Field Museum of Natural History Bird Collection	right	none
Ichthyornis dispar	fossil	Bhullar Lab	Michael Hanson	left	none
Iguana iguana	extant outgroup	MorphoSource	Ohio University Vertebrate Collection	right	none
*In ga**	fossil	Bhullar Lab	Anjan Bhullar	right	none
Majungasaurus crenatissimus	fossil	Morphosource	Field Museum of Natural History Fossil Herps Collection	left	none
Menura novaehollandiae	extant bird	MorphoSource	Field Museum of Natural History Bird Collection	right	none
Nestor notabilis	extant bird	MorphoSource	Field Museum of Natural History Bird Collection	right	none
Pandion haliaetus	extant bird	MorphoSource	Field Museum of Natural History Bird Collection	right	none
Podargus strigoides	extant bird	MorphoSource	Field Museum of Natural History Bird Collection	right	none
Prolacerta broomi	fossil	Bhullar Lab	Caleb Gordon	right	none
Sphenodon punctatus	extant outgroup	MorphoSource	Florida Museum of Natural History	right	segmented from CT data
Struthio camelus	extant bird	Bhullar Lab	Yale Peabody Museum	right	segmented from CT data
Velociraptor mongoliensis	fossil	Bhullar Lab	Caleb Gordon	right	none

*unpublished

Landmarking

Though many approaches to assigning landmarks have recently gained traction, including semilandmark curves, surface semilandmarks, and networks, it has been debated how well these interpolative techniques truly represent homology (e.g., Gonzalez et al., 2016; Palci & Lee, 2018). To avoid this potential problem and because we were primarily interested in functionally significant anatomy, we employed a scheme using only fixed landmarks, which are each manually and intentionally placed on a biologically relevant homologous point (Fig. 3). This technique provides greater control over and transparency in data collection, potentially reducing error. We designed a scheme of 21 fixed landmarks chosen to represent biologically significant features homologous across very disparate quadrate states, reconciling literature using different terminologies for fossil and extant traits (Table 2). These landmarks fall into four categories: those describing the morphology of the mandibular articulation, otic condyles, pterygoid and lateral flanges, and overall shape of curves. Where data was missing either due to incomplete fossil preservation or due to morphological overprinting of traits, fixed landmarks were estimated. All landmarks were digitized in the "geomorph" package in R by importing .ply bone models and manually selecting each landmark point on each quadrate (Adams & Otárola-Castillo, 2013). For left quadrates, landmark coordinates were reflected in the appropriate dimension after digitization.

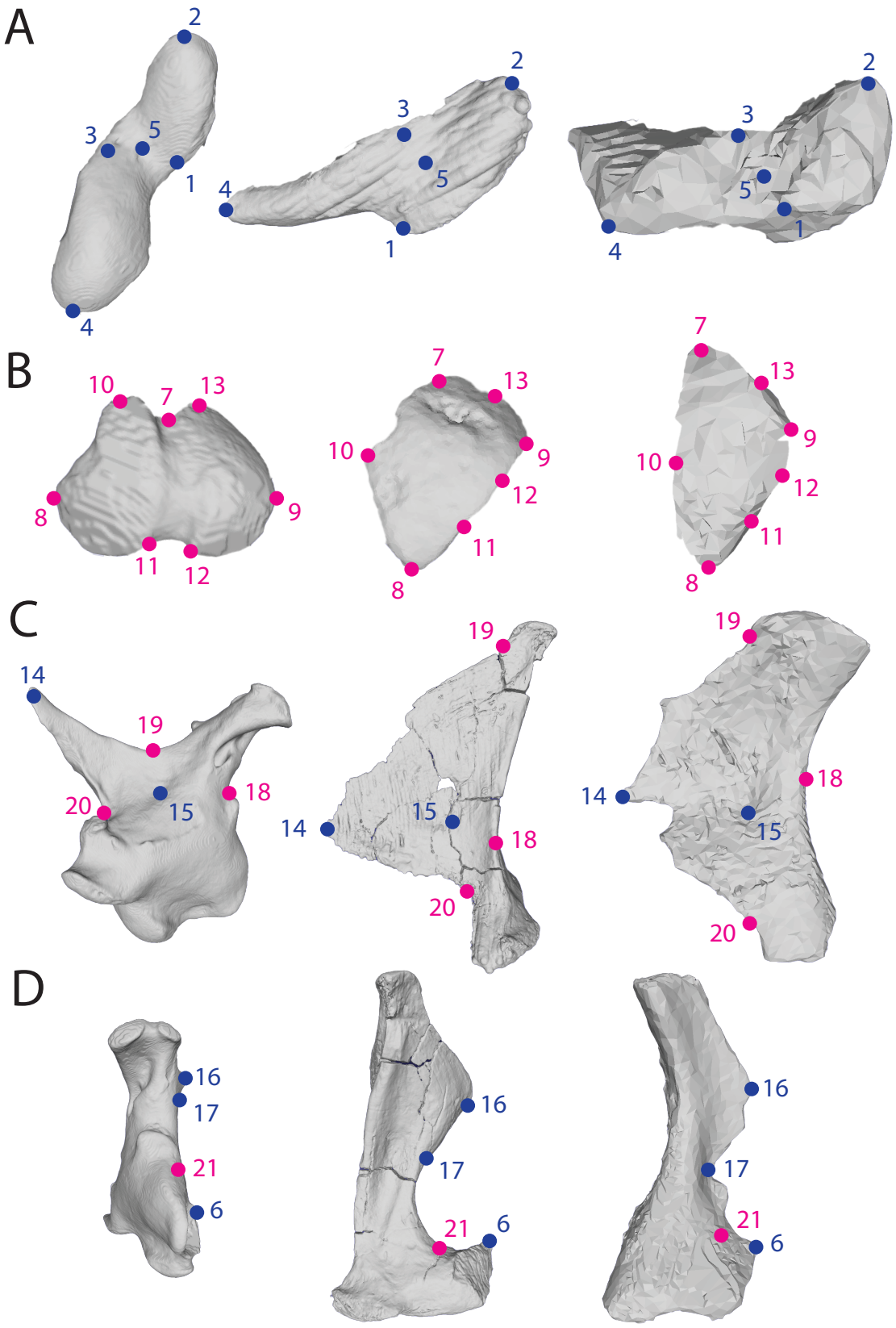
A
2
3
5
1
4
2
3
5
1
4
2
3
5
1
4
B
10
7
13
8
9
11
12
7
13
10
9
12
11
8
7
13
9
10
12
11
8
C
14
19
20
15
18
19
14
15
18
20
19
18
14
15
20
D
16
17
21
6
16
17
21
6
16
17
21
6

Fig. 3: Landmark positions of homologous points on the right quadrates of *Anas platyrhynchos* (left), *Velociraptor mongoliensis* (middle), and *Prolacerta broomi* (right). Quadrates are shown in ventral (A), dorsal (B), medial (C), and posterior (D) views, where anterior = top for ventral and dorsal views, anterior = left for medial view, and medial = left for posterior view. Landmarks are categorized as belonging to the mandibular articulation (navy), otic condyles (pink), pterygoid and lateral flanges (navy), or overall shape of curves (pink). Descriptions of landmarks by number are recorded in Table 2.

Table 2: Fixed landmark definitions.

Landmark	Description	Category
1	Posterior point of medial articular condyle (entocondyle)	Mandibular Articulation
2	Anterior point of medial articular condyle (entocondyle)	Mandibular Articulation
3	Anterior point of lateral articular condyle (ectocondyle)	Mandibular Articulation
4	Posterior point of lateral articular condyle (ectocondyle)	Mandibular Articulation
5	Deepest point of intercondylar sulcus	Mandibular Articulation
6	Distolateral extent of ventral quadratojugal process	Mandibular Articulation
7	Central anterior point of quadrate head	Otic Condyles
8	Posteromedial point of quadrate head	Otic Condyles
9	Posterolateral point of quadrate head	Otic Condyles
10	Anteromedial point of medial otic condyle (otic capitulum)	Otic Condyles
11	Posterolateral point of medial otic condyle (otic capitulum)	Otic Condyles
12	Posteromedial point of lateral otic condyle (squamosal capitulum)	Otic Condyles
13	Anterolateral point of lateral otic condyle (squamosal capitulum)	Otic Condyles
14	Distal extent of pterygoid flange (orbital process)	Pterygoid and lateral flanges
15	Medial fossa of the quadrate	Pterygoid and lateral flanges
16	Distal extent of lateral flange of the quadrate	Pterygoid and lateral flanges
17	Ventral contact between lateral flange and quadrate body	Pterygoid and lateral flanges
18	Inflection point of posterior concavity	Overall shape of curves
19	Dorsal contact between pterygoid flange and quadrate body (inflection point of dorsal concavity)	Overall shape of curves
20	Ventral contact between pterygoid flange and quadrate body (inflection point of ventral concavity)	Overall shape of curves
21	Dorsal contact between quadratojugal process and quadrate body (inflection point of lateral concavity in posterior view; “shoulder” of quadratojugal process)	Overall shape of curves

Analyses

We performed a generalized Procrustes analysis to normalize all datasets by position, size, and rotation, leaving only shape information, using the "gpagen" function in "geomorph" (Gower, 1975; Rohlf & Slice, 1990). This generates Procrustes coordinates, which were used for all subsequent analyses. We then performed a principal component analysis (PCA) on this dataset to summarize shape change in two dimensions for visualization, where the x-axis represents the most significant composite variable and the y-axis represents the second most significant composite variable. The amount of total shape variation represented by each principal component and the contribution of individual landmarks to principal components (rotations) were also extracted in R (Table 3). To visualize the "average" quadrate and the extremes of principal components 1 and 2, we identified the specimen closest to the dataset average and warped its quadrate mesh to the landmark coordinates of the average, PC1 maximum, PC1 minimum, PC2 maximum, and PC2 minimum.

Phylogenetic information was incorporated by directly projecting a phylogenetic tree onto the PCA as well as performing phylogenetic principal component analysis ("phyloPCA") to minimize and phylogenetically aligned component analysis ("PaCA") to maximize phylogenetic signal (Revell, 2009; Collyer & Adams, 2020). Phylogenetic PCA corrects for non-independence in interspecific analysis while PaCA aligns variation with phylogenetic signal; both are useful in understanding the relative importance of phylogenetic relationships on PCA results, especially in combination. Phylogenetic trees were created manually in Mesquite and exported as .nex files, then manipulated in R with the packages "ape" and "ggtree" (Maddison & Maddison, 2023; Paradis et al., 2004; Yu et al., 2016). Ancestral state PCA, phyloPCA, and PaCA coordinates were calculated and plotted, and selected ancestral state landmark coordinates were used to

create warped-mesh visualizations. All analyses were performed for the total dataset and for a subset of the data containing only crown birds.

RESULTS

XROMM results

Where the original publication of this dataset recorded overall motion of the quadrate with respect to the skull, our segmentation allowed for a more atomized analysis of specific articular interactions between bones during cranial kinesis. In addition to the mandibular bending noted by Dawson et al. (2011), our data indicate bending of the thin jugal bar, which comprises the jugal distally and the quadratojugal proximally. All three markers in the jugal bar are located proximally in the quadratojugal, which appears to behave as a rigid body based on the consistency of measured marker-to-marker distances. However, when the entire jugal bar is animated rigidly, the distalmost point of the jugal moves relative to the upper bill, though we know these elements are united in a fixed articulation. This is strong evidence for bending of the thin, unmarked, distal jugal during cranial kinesis, which complicates the traditional model of the cranial kinetic apparatus as a rigid four-bar linkage. In our animation, we represent the bending distal portion of the jugal bar as a dynamic line segment of variable length. We also observe motion at the quadrate-quadratojugal articulation, a joint whose motion is largely unstudied.

The joint coordinate system at the nasofrontal hinge reveals that, unsurprisingly, motion at this joint is dominated by pitching rotation about the mediolateral z-axis (Fig. 4A). At the quadrate-mandible joint, motion is similarly dominated by rotation about the mediolateral z-axis but is more complex, with significant rotation about the dorsoventral y-axis that has roughly the same frequency as the major rotation. The upper bill moves up and down about the axis of its

long hinge, while the mandible, connected to the skull by a smaller and less unidirectional contact, relies on mediolateral in addition to dorsoventral rotation in the recorded functional behavior. In this trial, the direction of the y-axis relative to the z-axis rotation is primarily opposite, with a positive z-axis rotation corresponding to a negative y-axis rotation and vice versa. Thus, in the majority of feeding cycles, the mandible appears to move clockwise in anterior view relative to the quadrate (Fig. 4D). However, there is some variability in the timing of y-axis rotation during the trial such that sometimes this relationship is reversed, resulting in a counterclockwise feeding cycle in anterior view and in-phase y-axis and z-axis rotations. This observation builds on those of Dawson et al. (2011) who treat the mandibular joint as a hinge with only z-axis rotation. For both the nasofrontal and mandibular articulations, rotation about the anteroposterior x-axis is relatively minimal.

Like Dawson et al. (2011), we find all three rotations of the otic joint at the quadrate-squamosal articulation to contribute significantly to overall motion during cranial kinesis, using a joint coordinate system based on the anatomy of the otic joint. Our results are also in agreement with the timing observed by Dawson et al. (2011), where motion of the upper and lower bills is mechanically coupled by a shared origin at the quadrate, though enacted by different anatomical mechanisms. In a single feeding cycle from a completely closed to completely open gape, the quadrate moves first, initiating a rotation positively about the dorsoventral y-axis and negatively about the mediolateral z-axis relative to the braincase, with the orbital process moving dorsomedially relative to the otic process. The beginning of this motion is followed by anteriorward motion of the jugal bar and rotation at the mandibular articulation such that motion at the otic joint, mandibular joint, and nasofrontal hinge occur simultaneously. In addition to the relative timing of upper and lower bill motion, we find the movement of the jugal bar, an internal

component of the system, to be coupled with quadrate motion. At the quadrate-quadratojugal joint, the jugal bar moves in the ventral direction relative to the quadrate, significantly increasing the angle between the orbital process of the quadrate and the jugal bar at full gape (Fig. 4B).

During the transition from closed to open gape, rotation at the otic joint appears to rely mostly on the dorsally facing lateral otic condyle rather than the posteriorly facing medial otic condyle. Over the course of the cycle, the articular surface of the medial condyle moves away from its corresponding articular surface on the squamosal, while the lateral condyle remains in broad contact with the squamosal throughout. As the quadrate swings simultaneously forward and inward, the main point of contact between the lateral condyle and the squamosal shifts from the posterior to anterior portion of the articular surface of the lateral condyle, such that every part of the articular surface of the lateral condyle comes into contact with the squamosal at some point during the cycle (Fig. 4C). At the maximal extent of the gape, where both the nasofrontal hinge and mandibular articulation show their highest rotation value of the cycle, the anteriormost edge of the articular surface of the lateral condyle is in contact with the squamosal and the medial condyle is uninvolved in the articulation. However, the medial condyle is used when the gape is closed, i.e., when cranial kinesis is not occurring. The rotation pattern described here can be most clearly seen during the cycles of widest gape. For cycles of smaller amplitude, corresponding to food processing rather than food acquisition, rotations in all three dimensions are about equally significant and the entire lateral condyle articular surface is not necessarily used, though an inverse relationship between the y-axis and z-axis rotations is preserved. X-axis rotation is generally in phase with z-axis rotation, though the fidelity of this relationship is variable over the course of the trial.

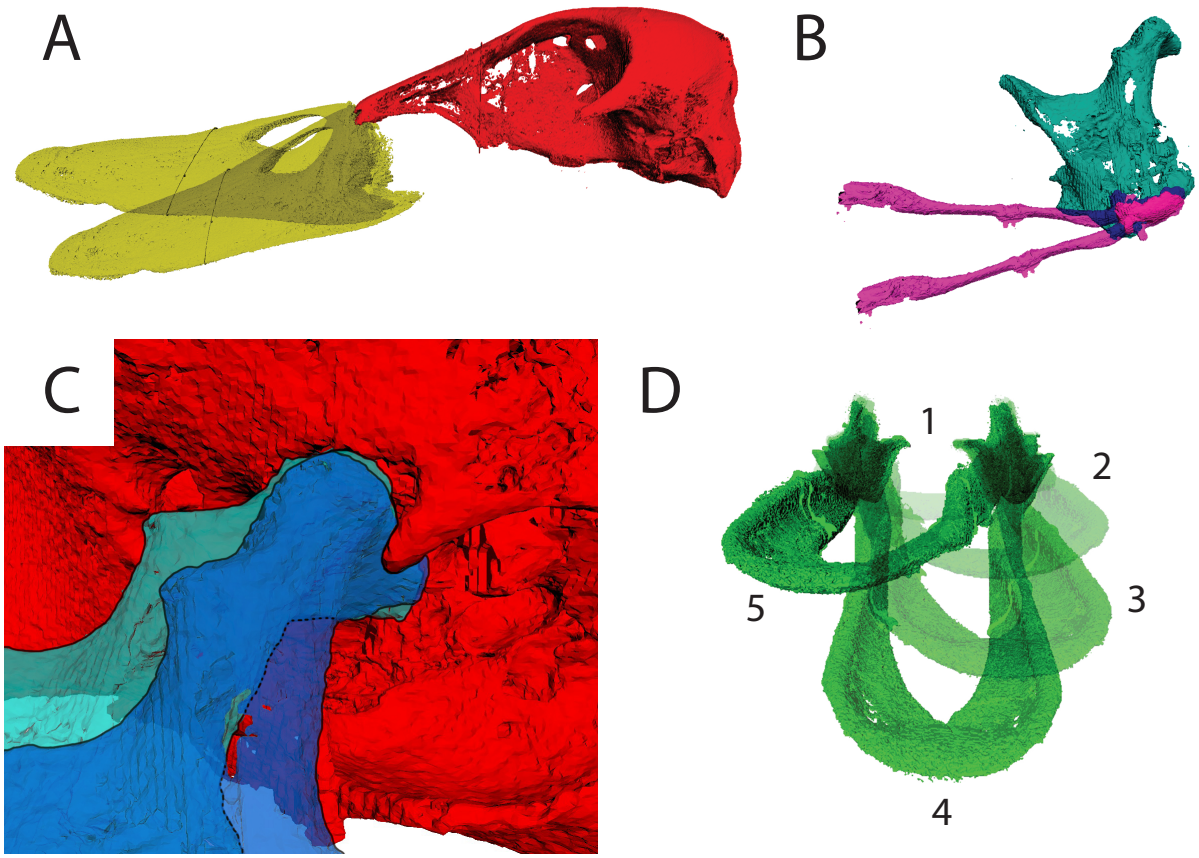

Fig. 4: Images from the XROMM animation, overlaid at different time points. Extent of z-axis rotation about the nasofrontal hinge (A), increased quadrate-quadratojugal angle during open gape (B), and range of motion of the otic joint at the quadrate-squamosal articulation (quadrate in blue, braincase in red) (C), all in left lateral view from XROMM frames 1615 and 1652. The mandible opens clockwise in anterior view with respect to the quadrate (positions during one cycle progress from 1-5) (D).

GM results

Our PCA results confirm qualitative observations of an abrupt transition from the ancestral to derived general quadrate morphology along the avian lineage (Fig. 5). All nonavian reptiles have a negatively shifted PC 1 value relative to modern birds, with the exception of *Colibri coruscans*, a hummingbird with a distinctly primitive-looking pterygoid flange/orbital process (see Fig. 2). The ornithurine *Hesperornis regalis* plots within the convex hull of modern bird morphospace, with the slightly earlier diverging ornithurine *Ichthyornis dispar* on the edge of this convex hull; this result confirms the prior interpretation of ornithurine quadrate morphology as essentially modern (Fig. 5). In this analysis, PC 1 accounts for 39.2% of the variance and primarily represents the contributions of the pterygoid flange/orbital process (landmarks 19 and 14), the lateral flange (landmark 17), and the anterolateral mandibular condyle (landmark 3) (Table 3). Change along this axis, visualized using warped meshes of the *Iguana iguana* quadrate, shows a major transformation to an anterioposteriorly longer pterygoid flange/orbital process coupled with a relative shrinking of the lateral flange and a widening of the mandibular condyles, causing an overall change in long-axis orientation of the bone (Fig. 5A). PC 2 accounts for 8.6% of the variance and primarily represents the contributions of the pterygoid flange/orbital process (landmark 14), the lateral flange (landmark 17), the quadrate head (landmark 8), and the anteriomedial mandibular condyle (landmark 2) (Table 3). Change along this axis also reflects a transformation toward a larger pterygoid flange/orbital process, here with an overall expansion of the lateral surface of the quadrate and less reorientation (Fig. 5A). Though landmark 14, representing the distal extent of the pterygoid flange, may be having an outsized impact on our PCA, we believe based on qualitative evidence that this is truly the region of most significant morphological change over nonavian-to-avian quadrate evolution.

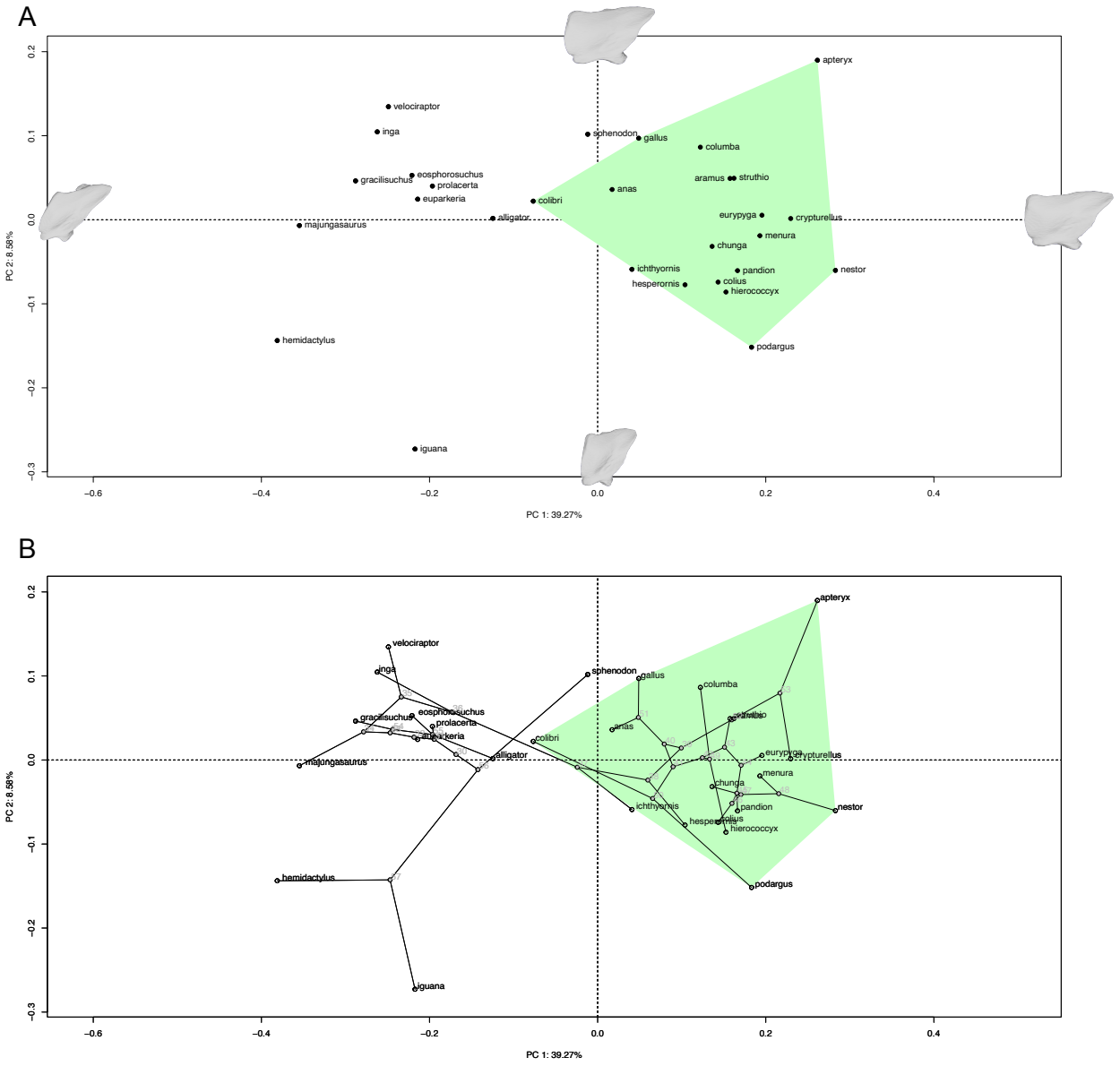

Fig. 5: PCA results for the full sample without (A) and with (B) projected phylogeny. Extant birds, in green, occupy positively shifted PC 1 values compared to non-avian reptiles. Warped right quadrate meshes represent PC 1 and PC 2 extremes, shown in lateral view (anterior = right).

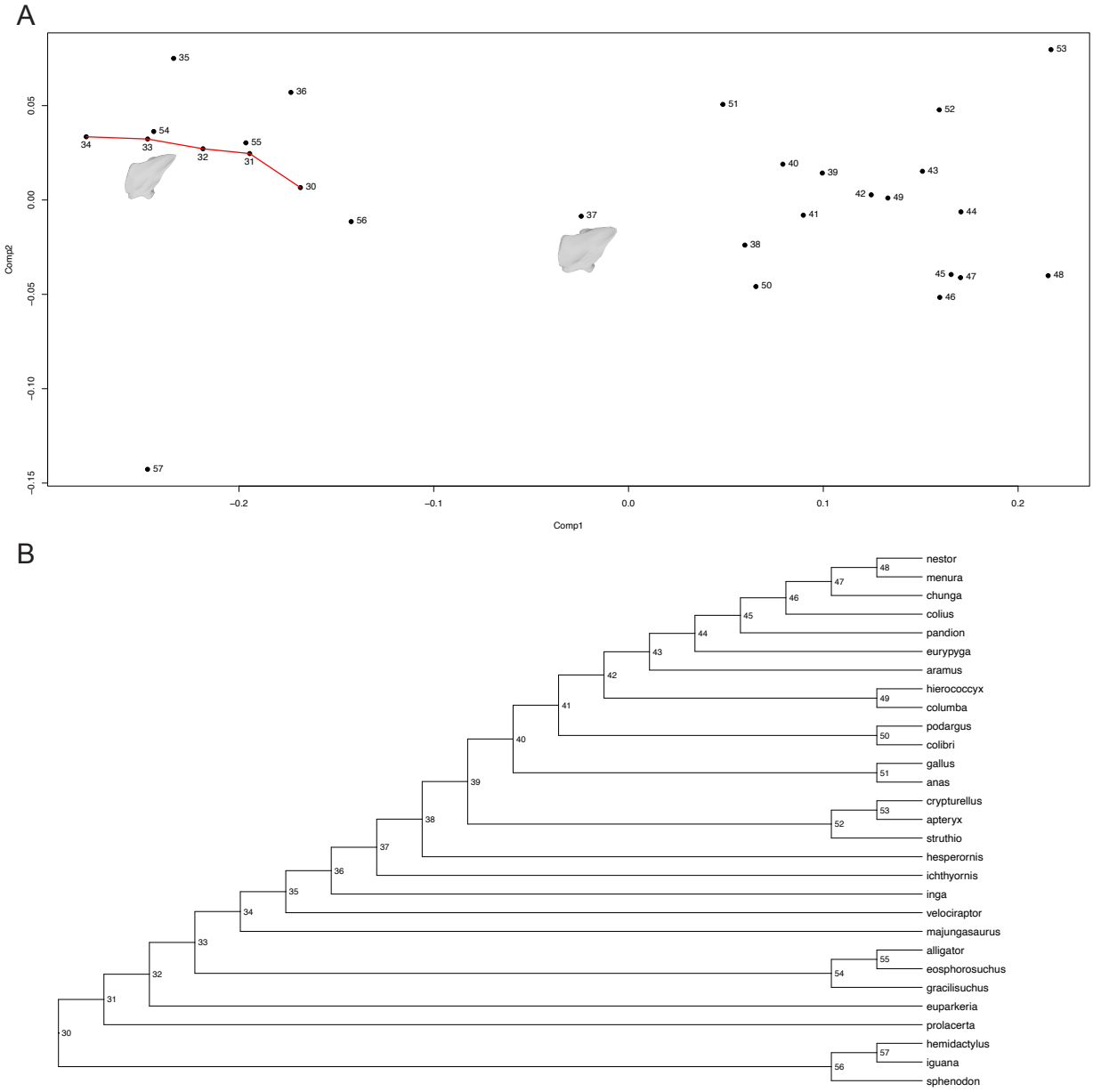

Fig. 6: PCA of ancestral states (A) and node label definitions (B). Evolutionary trajectory down PC 1 from the root (30) to archosauromorph (31), archosauriform (32), archosaur (33), and avemetatarsalian (34) ancestral states shown in red. Node 37 represents the ornithurine ancestral state, the transition to modern avian quadrate morphologies. Warped right quadrate meshes of the ancestral archosaur and ornithurine conditions in lateral view (anterior = right).

Table 3: Landmark contributions to principal components 1 and 2 for the full analysis and the extant bird subset.

Full Analysis				Extant Bird Subset			
PC	**Landmark**	**Vector Direction**	**Rotation Coefficient**	**PC**	**Landmark**	**Vector Direction**	**Rotation Coefficient**
1	19	X	0.446915626	1	3	Y	0.390104988
1	14	Y	-0.394648027	1	4	Z	-0.337197517
1	17	X	-0.331675726	1	6	Z	0.30419629
1	3	Y	0.209570712	1	3	X	0.303833181
1	19	Y	-0.207020493	1	4	X	0.296487293
2	14	X	0.464078865	2	2	Y	0.538858554
2	14	Z	-0.280785247	2	1	Y	-0.397944248
2	17	Y	-0.261295753	2	14	Y	-0.284379514
2	8	X	-0.214393681	2	1	Z	-0.221931894
2	2	Y	0.196880604	2	2	Z	0.209349453

Our results also capture, for the first time, the evolutionary trajectory of quadrate morphology leading up to the sudden transformation. PCA results show a clear progression from the basal archosauromorph state (represented by *Prolacerta broomi*) down PC 1 to an ancestral archosaur condition, followed by a trend up PC 2 to an ancestral paravian condition (Fig. 6A). Even at low resolution, this pattern of quadrate evolution predating any modern morphology shows that the element was already experiencing directional evolution along similar morphological axes before the innovation of the modern configuration.

PhyloPCA reaffirms the division between ancestral and derived morphologies, independent of phylogeny. The only major changes in this analysis compared to the original PCA are the splitting of the lepidosaur outgroup clade and of the pseudosuchian clade, with birds and close bird relatives generally maintaining a tighter cluster at high PC 1 values. Though paleognaths are split from one another and *Colibri* is still unusually low on PC 1, this general trend indicates that in our sample, independent of phylogenetic signal, the bird quadrate is relatively conserved compared to the lepidosaur and pseudosuchian quadrates. Alternatively, maximizing phylogenetic signal using PaCA leads to even more pronounced isolation between the clusters of bird and non-bird quadrates. In both phyloPCA and PaCA analyses, *Ichthyornis*

and *Hesperornis* fall inside the extant bird convex hull, indicating the consistently modern placement of their quadrate morphologies.

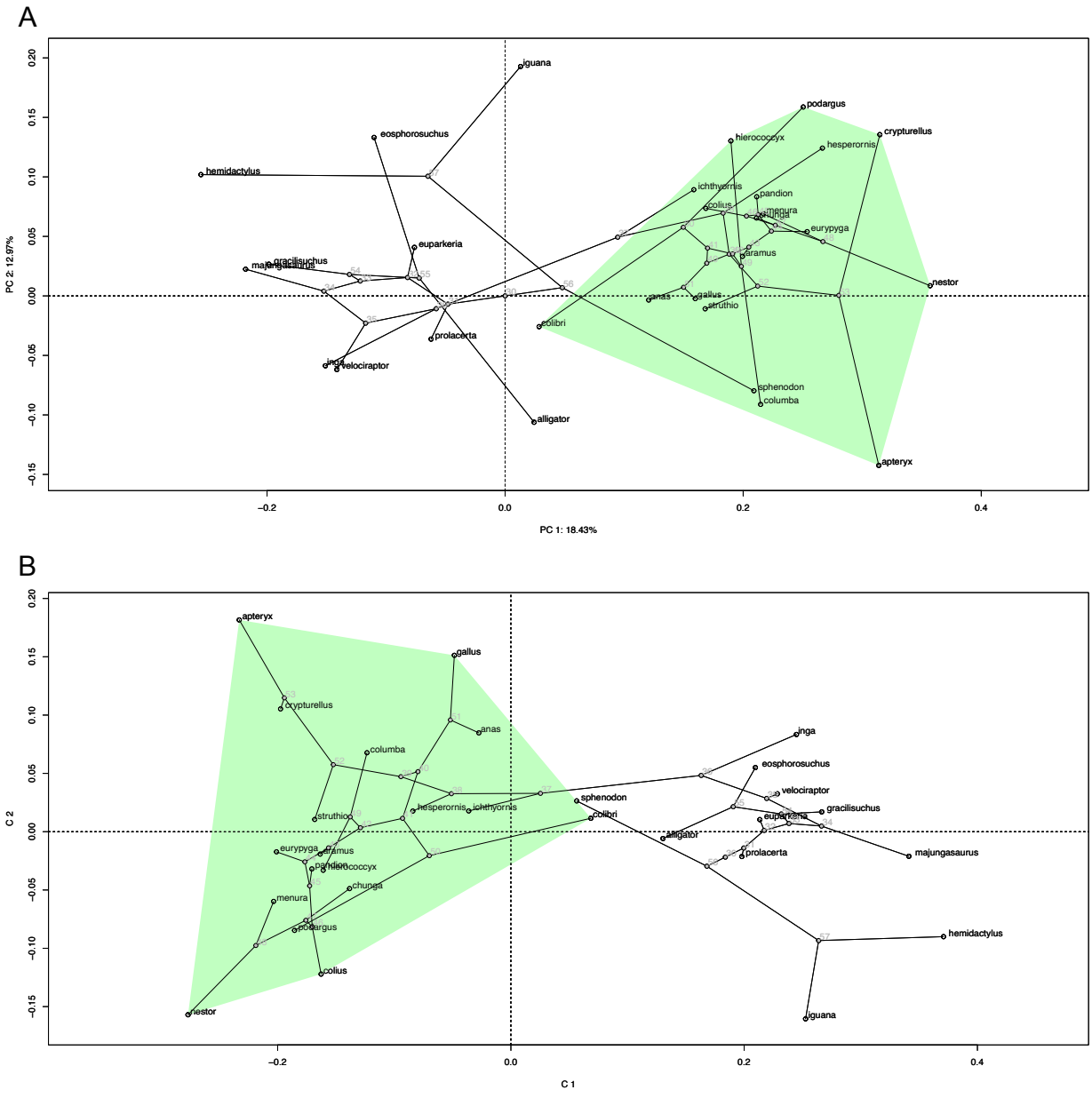

Fig. 7: Both phyloPCA (A) and PaCA (B) results show a cluster of modern birds (green), indicating a notable morphological difference between the ancestral and derived quadrate conditions regardless of relatedness.

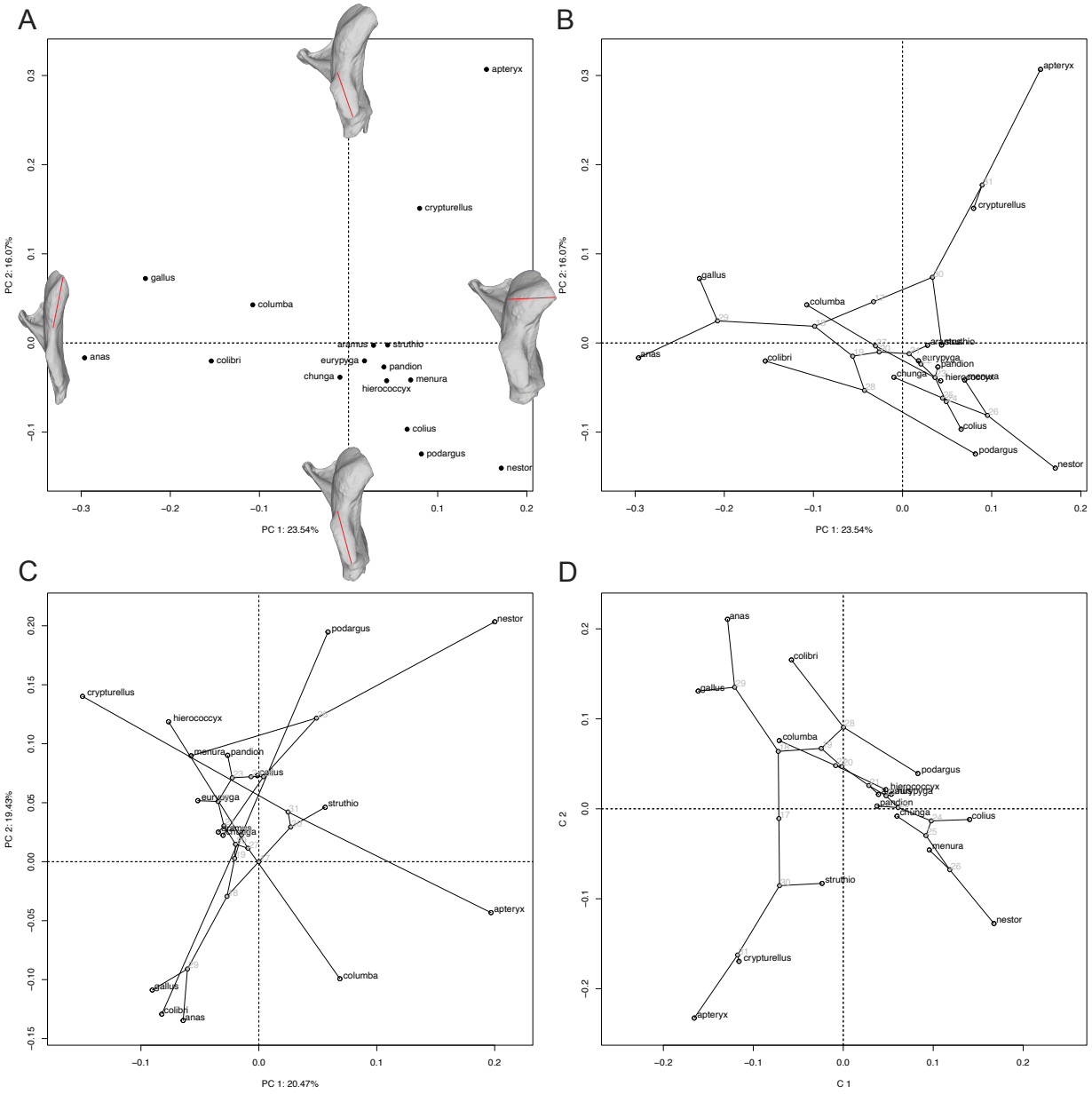

Fig. 8: PCA without (A) and with (B) projected phylogeny, phyloPCA (C), and PaCA (D) for the extant bird subset of the data. Warped meshes in ventral view (top = posterior) show a change in the orientation of the long axis of the lateral mandibular condyle along PC 1 and in the length of the long axis of the medial mandibular condyle along PC 2 (long axes shown in red). The difference between the cluster structure of the phyloPCA plot and the tree structure of the PaCA plot shows a strong phylogenetic signal.

Within modern birds, our PCA analysis shows relatively high disparity among paleognaths, particularly high PC 2 values for *Crypturellus undulatus* and *Apteryx australis*. Galloanserans have the lowest PC 1 values. Using the modern bird subset of the data, PC axes are mainly influenced by the morphology of the mandibular articulation, with PC 1 (23.5% of the variance) representing the change in the lateral condyle (landmarks 3, 4, 6) while PC 2 (16.1% of the variance) represents the change in the medial condyle (landmarks 1 and 2) as well as the extent of the orbital process (landmark 14) (Table 3). Right quadrate meshes warped to the maximum and minimum values of PC 1 show that an increase along PC 1 represents a shift from a narrow, anteroposteriorly elongate lateral condyle to a rounded lateral condyle with a roughly mediolateral long axis (Fig. 8A). An increase along PC 2 represents an anteroposterior shortening of the medial condyle without reorientation of the long axis (Fig. 8A). The phyloPCA and PaCA analyses of the extant bird subset look quite different, indicating a strong phylogenetic signal in the data. PhyloPCA highlights the disparity of paleognaths *Crypturellus* and *Apteryx* and galloanserans *Gallus varius* and *Anas platyrhynchos* as compared to the rest of the sample. *Colibri*, mentioned above, clusters with the galloanserans, while *Columba livia*, *Podargus strigoides*, and *Nestor notabilis* are other outliers from the large central cluster. The linearity of the PaCA tree confirms a strong phylogenetic relationship: paleognaths have low PC 2 values, galloanserans have high PC 2 values, and neoaves have high PC 1 values. *Nestor*, a parrot with extreme cranial kinesis ability, is an outlier in all three analyses. We do not observe any clear ecological signal in the modern results.

DISCUSSION

This paper represents the first map of the quadrate's evolutionary trajectory from basal archosauromorph to bird. We show that the quadrate experienced directional morphological

change prior to the sudden innovation of the modern condition. The conservation of axes (representing composite anatomical variables) that capture both gradual and sudden change indicates that the bird-line quadrate has a long history of morphological evolution of the features important to modern cranial kinetic function.

In particular, the changing roles of homologous structures with respect to articulations between the quadrate and surrounding musculoskeletal tissues provided a pathway to new functional ability. Both PC 1 and PC 2 of our full analysis implicate the lateral flange's contribution to morphological disparity. This process of the quadrate, absent in modern birds, is the site of a dorsal articulation with the quadratojugal in many fossil taxa and in *Sphenodon*. In the ancestral state, the lateral flange functions to bound the middle ear cavity and support the tympanum, suggesting that functional selection on hearing might have been a driver of evolutionary changes to this structure along the avian lineage prior to the major quadrate transformation. Then, the reduction of the lateral flange in all ornithurines caused the quadrate and quadratojugal to be linked only by a single, ventrally located joint, a joint which our XROMM results show to be mobile during cranial kinesis. Thus, existing patterns of quadrate evolution along the ancestral lineage contributed to novel functional opportunities.

Additionally, the morphology of the mandibular condyles significantly contributes to the principal components of both our full analysis and our bird-only analysis. We find the ancestrally bicondylar mandibular articulation to be a major source of disparity in modern birds, where the medial condyle may variably be co-opted to contribute to the pterygoid process (e.g., in ducks) or an expanded ventral quadratojugal process may contribute to the mandibular articulation (e.g., in *Chunga burmeisteri*). The redundancy of the ancestral mandibular condyles allows evolutionary opportunity for a variety of functionally diverse morphologies in modern birds.

From our XROMM results, the morphology of the mandibular articulation allows for complex functional behaviors like the coupled y-axis and z-axis rotations that give modern ducks an anteriorly clockwise feeding cycle. In the quadrate's articulations with both the quadratojugal and the mandible, morphologically homologous structures are not functionally equivalent between the ancestral and derived states, or even among variations on the modern condition.

Further, a synthesis of our XROMM and GM analyses illuminates the role of the bicondylar otic joint of the quadrate in kinetic function. Observations from our XROMM data indicate that the dorsally facing lateral otic condyle is more significant in enabling kinesis than the posteriorly facing medial otic condyle in ducks, and show a differential role for these two condyles in closed-gape vs. open-gape positions. Since the entire articular surface of the lateral condyle seems to be used, its morphology may be functionally predictive. Once again, the evolution of articular surfaces involved in the otic joint is precedented in the fossil record. Change in the position of the posteromedial point of the quadrate head is captured by PC 2 in our full GM analysis (Table 2, 3), which shows a positive shift from the ancestral archosaur to the dinosaur state and variability among crown birds. This result indicates a change in evolutionary pattern from directional evolution of the quadrate head along the avian lineage to diversification among modern otic joints.

The drastic disparity of the otic joint within neoaves suggests that, like at the mandibular articulation, the redundancy of the bicondylar otic joint may contribute to functional diversity. Our sample reveals major differences in the size and position of the two otic condyles relative to each other: in some neoaves, the lateral condyle dominates (e.g., *Hierococcyx fugax*, *Colius macrourus*), in others, the medial condyle dominates (e.g., *Aramus guarauna*, *Menura novaehollandiae*), and in others, both appear to contribute equally (e.g., *Eurypyga helias*). This

diversity is less pronounced in the paleognaths and galloanserans included in our sample and does not apply at all to some paleognaths with a unicondylar quadrate head (*Crypturellus undulatus*, *Struthio camelus*). Thus, as a relatively basal form with less differentiated condyles than in many other taxa, duck otic joint anatomy is probably a conservative window into the potential subfunctionalization of the two otic condyles during kinesis. Future *in vivo* analyses with a broader sample would be valuable in determining the relationship between otic joint disparity and complex streptostylic behavior. For instance, paleognaths have a distinct kinetic mechanism as compared to neognaths and some possess a single otic condyle; more data is required to determine whether these phenomena are related.

This study also opens a new area of investigation into the jugal's role in avian cranial kinesis. Previous research on extant birds has focused on the palate more than the jugal as a conduit for quadrate motion to the craniofacial hinge. In parallel, fossil evidence is biased toward the jugal rather than the palate, since fossils are commonly preserved in lateral view with the palate obscured or destroyed. A thin, "rod-like" jugal has been cited as a morphological prerequisite for cranial kinesis in the fossil stem-bird *Shuvuuia* (Chiappe et al., 1998), and a comparative description of the jugals and quadratojugals of bird-line fossils postulated that the jugal bar's derived overall shape and reduced articulation with other elements contributes to cranial kinesis potential (Wang & Hu, 2016). Though the functional importance of the jugal bar to kinesis has not yet been fully explored, our XROMM results provide the first significant evidence that this element is flexible during cranial kinesis in ducks. Furthermore, our observed jugal bending combined with previously reported mandibular bending may call for a reconsideration of rigid body calculations in XROMM, possibly requiring new best practices for

marker insertion in flexible elements or the development of new methods for higher-fidelity animation of bone deformation.

Future Directions

Avian cranial kinesis is a powerful system for studying the relationship between morphological and functional modularity, or the extent to which groups of bones evolve and/or function as a unit (Zelditch & Goswami, 2021). Concepts of modularity among biological subfields are not equivalent but are often assumed so based on an understanding that natural selection on a functional unit will necessarily result in coevolution of the elements involved. An approach like this one that synthesizes paleontological and biomechanical methods and data may provide a unique opportunity to explore the validity of this assumption.

CONCLUSION

Through a combination of *in vivo* XROMM analysis of cranial kinesis in a living duck and fixed-landmark 3D GM analysis of quadrate bones along the avian stem from archosauromorphs to crown birds, we find that evolutionary changes in the quadrate's articulations with surrounding bones are of functional significance. Movement at the quadrate-quadratojugal joint and a flexible jugal bar contribute to the kinetic apparatus, enabled by the disappearance of the ancestral lateral flange and therefore a reduction in total articular contact between the quadrate and the quadratojugal. Modern mandibular condyle morphology allows for complex jaw rotation during duck feeding including coupled y-axis and z-axis rotations. This motion is likely diverse among living birds, who possess a wide range of mandibular condyle morphology enabled by the redundancy of the ancestral bicondylar mandibular joint, where either condyle may dominate in the modern avian condition. Finally, the otic joint between the

quadrate head and the squamosal is a rare case of a bone-bone interaction that transforms evolutionarily from a static articulation to a highly mobile joint. The bicondylar nature of this joint, which allows for a wide range of motion during duck feeding behavior as the medial otic condyle dominates during closed-gape positions while the lateral otic condyle dominates during open-gape positions, is a key innovation of derived modern birds and functionally significant for kinesis. Archosaur quadrate morphological evolution progressed along these same anatomical dimensions in deep time, but sudden transformations with functional significance allowed the modern quadrate to quickly gain dominance and aid birds in their Cenozoic success.

ACKNOWLEDGEMENTS

This project was made possible by the XROMM dataset contributed by Dr. Elizabeth Brainerd and the fossil datasets contributed by Dr. Michael Hanson, Caleb Gordon, and Alex Ruebenstahl. This project is co-authored by Dr. Bhart-Anjan Bhullar and Dr. Armita Manafzadeh, my longtime mentors who have provided immense intellectual contributions both to this thesis and to my study of paleontology. Thank you also to my second reader Dr. Jacques Gauthier, my mentors and research advisors Dr. Derek Briggs and Dr. Pincelli Hull, and members of the Bhullar Lab, Yale Peabody Museum, and Yale Earth and Planetary Sciences communities who have provided guidance and support.

REFERENCES

Adams, D. C., & Otárola-Castillo, E. (2013). Geomorph: An R package for the collection and analysis of geometric morphometric shape data. *Methods in Ecology and Evolution*, *4*(4), 393–399. https://doi.org/10.1111/2041-210X.12035

Bailleul, A. M., Witmer, L. M., & Holliday, C. M. (2017). Cranial joint histology in the mallard duck (*Anas platyrhynchos*): New insights on avian cranial kinesis. *Journal of Anatomy*, *230*(3), 444–460. https://doi.org/10.1111/joa.12562

Bhattacharyya, B. N. (2013). Avian jaw function: Adaptation of the seven-muscle system and a review. *Proceedings of the Zoological Society*, *66*(2), 75–85. https://doi.org/10.1007/s12595-012-0056-x

Bhullar, B.-A. S., Hanson, M., Fabbri, M., Pritchard, A., Bever, G. S., & Hoffman, E. (2016). How to make a bird skull: Major transitions in the evolution of the avian cranium, paedomorphosis, and the beak as a surrogate hand. *Integrative and Comparative Biology*, *56*(3), 389–403. https://doi.org/10.1093/icb/icw069

Bhullar, B.-A. S., Manafzadeh, A. R., Miyamae, J. A., Hoffman, E. A., Brainerd, E. L., Musinsky, C., & Crompton, A. W. (2019). Rolling of the jaw is essential for mammalian chewing and tribosphenic molar function. *Nature*, *566*(7745), 528–532. https://doi.org/10.1038/s41586-019-0940-x

Brainerd, E. L., Baier, D. B., Gatesy, S. M., Hedrick, T. L., Metzger, K. A., Gilbert, S. L., & Crisco, J. J. (2010). X-ray reconstruction of moving morphology (XROMM): Precision, accuracy and applications in comparative biomechanics research. *Journal of Experimental Zoology Part A: Ecological Genetics and Physiology*, *313A*(5), 262–279. https://doi.org/10.1002/jez.589

Bühler, P., Martin, L. D., & Witmer, L. M. (1988). Cranial kinesis in the Late Cretaceous birds *Hesperornis* and *Parahesperornis*. *The Auk*, *105*(1), 111–122. https://doi.org/10.1093/auk/105.1.111

Chiappe, L. M., Norell, M. A., & Clark, J. M. (1998). The skull of a relative of the stem-group bird *Mononykus*. *Nature*, *392*(6673), 275–278. https://doi.org/10.1038/32642

Collyer, M. L., & Adams, D. C. (2021). Phylogenetically aligned component analysis. *Methods in Ecology and Evolution*, *12*(2), 359–372. https://doi.org/10.1111/2041-210X.13515

Dawson, M. M., Metzger, K. A., Baier, D. B., & Brainerd, E. L. (2011). Kinematics of the quadrate bone during feeding in mallard ducks. *Journal of Experimental Biology*, *214*(12), 2036–2046. https://doi.org/10.1242/jeb.047159

Elzanowski, A., & Stidham, T. A. (2010). Morphology of the quadrate in the Eocene anseriform *Presbyornis* and extant galloanserine birds. *Journal of Morphology*, *271*(3), 305–323. https://doi.org/10.1002/jmor.10799

Gonzalez, P. N., Barbeito-Andrés, J., D'Addona, L. A., Bernal, V., & Perez, S. I. (2016). Technical note: Performance of semi and fully automated approaches for registration of 3D surface coordinates in geometric morphometric studies. *American Journal of Physical Anthropology*, *160*(1), 169–178. https://doi.org/10.1002/ajpa.22934

Gower, J. C. (1975). Generalized procrustes analysis. *Psychometrika*, *40*(1), 33–51. https://doi.org/10.1007/BF02291478

Gussekloo, S. W. S., & Bout, R. G. (2005). The kinematics of feeding and drinking in palaeognathous birds in relation to cranial morphology. *Journal of Experimental Biology*, *208*(17), 3395–3407. https://doi.org/10.1242/jeb.01769

Gussekloo, S. W. S., Vosselman, M. G., & Bout, R. G. (2001). Three-dimensional kinematics of skeletal elements in avian prokinetic and rhynchokinetic skulls determined by Roentgen stereophotogrammetry. *Journal of Experimental Biology*, *204*(10), 1735–1744. https://doi.org/10.1242/jeb.204.10.1735

Hendrickx, C., Araújo, R., & Mateus, O. (2015). The non-avian theropod quadrate I: Standardized terminology with an overview of the anatomy and function. *PeerJ*, *3*, e1245. https://doi.org/10.7717/peerj.1245

Holliday, C. M., & Witmer, L. M. (2008). Cranial kinesis in dinosaurs: Intracranial joints, protractor muscles, and their significance for cranial evolution and function in diapsids. *Journal of Vertebrate Paleontology*, *28*(4), 1073–1088. https://doi.org/10.1671/0272-4634-28.4.1073

Kardong, K. V. (1977). Kinesis of the jaw apparatus during swallowing in the cottonmouth snake, *Agkistrodon piscivorus*. *Copeia*, *1977*(2), 338. https://doi.org/10.2307/1443913

Knörlein, B. J., Baier, D. B., Gatesy, S. M., Laurence-Chasen, J. D., & Brainerd, E. L. (2016). Validation of XMALab software for marker-based XROMM. *Journal of Experimental Biology*, jeb.145383. https://doi.org/10.1242/jeb.145383

Kuo, P., Benson, R. B. J., & Field, D. J. (2023). The influence of fossils in macroevolutionary analyses of 3D geometric morphometric data: A case study of galloanseran quadrates. *Journal of Morphology*, *284*(6), e21594. https://doi.org/10.1002/jmor.21594

Maddison, W. P. and D.R. Maddison. 2023. Mesquite: A modular system for evolutionary analysis. Version 3.81. http://www.mesquiteproject.org

Palci, A., & Lee, M. S. Y. (2019). Geometric morphometrics, homology and cladistics: Review and recommendations. *Cladistics*, *35*(2), 230–242. https://doi.org/10.1111/cla.12340

Paradis, E., Claude, J., & Strimmer, K. (2004). Ape: Analyses of phylogenetics and evolution in R language. *Bioinformatics*, *20*(2), 289–290. https://doi.org/10.1093/bioinformatics/btg412

Prum, R. O., Berv, J. S., Dornburg, A., Field, D. J., Townsend, J. P., Lemmon, E. M., & Lemmon, A. R. (2015). A comprehensive phylogeny of birds (Aves) using targeted next-generation DNA sequencing. *Nature*, *526*(7574), 569–573. https://doi.org/10.1038/nature15697

Revell, L. J. (2009). Size-correction and principal components for interspecific comparative studies. *Evolution*, *63*(12), 3258–3268. https://doi.org/10.1111/j.1558-5646.2009.00804.x

Rohlf, F. J., & Slice, D. (1990). Extensions of the Procrustes method for the optimal superimposition of landmarks. *Systematic Zoology*, *39*(1), 40. https://doi.org/10.2307/2992207

Tsai, H. P., Turner, M. L., Manafzadeh, A. R., & Gatesy, S. M. (2020). Contrast-enhanced XROMM reveals *in vivo* soft tissue interactions in the hip of *Alligator mississippiensis*. *Journal of Anatomy*, *236*(2), 288–304. https://doi.org/10.1111/joa.13101

Wang, M., & Hu, H. (2017). A comparative morphological study of the jugal and quadratojugal in early birds and their dinosaurian relatives. *The Anatomical Record*, *300*(1), 62–75. https://doi.org/10.1002/ar.23446

Wang, M., Stidham, T. A., O'Connor, J. K., & Zhou, Z. (2022). Insight into the evolutionary assemblage of cranial kinesis from a Cretaceous bird. *eLife*, *11*, e81337. https://doi.org/10.7554/eLife.81337

Weller, H. I., Olsen, A. M., Camp, A. L., Manafzadeh, A. R., Hernandez, L. P., & Brainerd, E. L. (2020). An XROMM study of food transport and swallowing in channel catfish. *Integrative Organismal Biology*, *2*(1), obaa018. https://doi.org/10.1093/iob/obaa018

Westneat, M. W. (2005). Skull biomechanics and suction feeding in fishes. In *Fish Physiology* (Vol. 23, pp. 29–75). Elsevier. https://doi.org/10.1016/S1546-5098(05)23002-9

Wilken, A. T., Sellers, K. C., Cost, I. N., Rozin, R. E., Middleton, K. M., & Holliday, C. M. (2020). Connecting the chondrocranium: Biomechanics of the suspensorium in reptiles. *Senckenberg Gesellschaft Für Naturforschung*. https://doi.org/10.26049/VZ70-3-2020-02

Yu, G., Smith, D. K., Zhu, H., Guan, Y., & Lam, T. T. (2017). GGTREE: An R package for visualization and annotation of phylogenetic trees with their covariates and other associated data. *Methods in Ecology and Evolution*, *8*(1), 28–36. https://doi.org/10.1111/2041-210X.12628

Zelditch, M. (Ed.). (2004). *Geometric morphometrics for biologists: A primer*. Elsevier Academic Press.

Zelditch, M. L., & Goswami, A. (2021). What does modularity mean? *Evolution & Development*, *23*(5), 377–403. https://doi.org/10.1111/ede.12390

Zusi, R. L. (1984). A functional and evolutionary analysis of rhynchokinesis in birds. *Smithsonian Contributions to Zoology*, *395*, 1–40. https://doi.org/10.5479/si.00810282.395

Zweers, G., & Berkhoudt, H. (2001). Ingestion in birds. In John Wiley & Sons, Ltd (Ed.), *eLS* (1st ed.). Wiley. https://doi.org/10.1038/npg.els.0001836